Design and Implementation of a Bi-Directional Charger for an 800V Electric Vehicle

Saajan Patel

Abstract

Fossil fuels are currently being phased out by many sectors to reduce greenhouse gas emissions to help preserve the current global climate. The energy sector could reduce its emissions by switching to renewable clean energy sources, while the transport sector could reduce emissions through the transition to battery electric vehicles (BEVs) technology. By acting as energy stores when idle, BEVs can aid the adoption of renewable clean energy sources and help reduce the cost of the energy sector's new infrastructure. Furthermore, owners of the BEVs could be financially compensated for their participation. The BEV would be connected to the grid through a bi-directional charger that could send or receive power. Due to current manufacturer trends, this report looked at the design and implementation of a bi-directional charger for an 800V BEV architecture. A charger model and its controllers were built in Simulink with the preliminary simulation results looking promising and offered a control systems to implement into a hardware testing.

Supervised by Dr. J. Wang
Department of Electrical and Electronic Engineering
University of Bristol
2022

Declaration

This project report is submitted towards an application for a degree in Mechanical and Electrical Engineering at the University of Bristol. The report is based upon independent work by the candidate. All contributions from others have been acknowledged and the supervisor is identified on the front page. The views expressed within the report are those of the author and not of the University of Bristol. I hereby assert my right to be identified as the author of this report. I give permission to the University of Bristol Library to add this report to its stock and to make it available for consultation in the library, and for inter-library lending for use in another library. It may be copied in full or in part for any bone fide library or research worker on the understanding that users are made aware of their obligations under copyright legislation.

I hereby declare that the above statements are true.

Saajan Patel

Contents

1 Introduction

The UK has seen a 9.5% decrease in its greenhouse gas (GHG) emissions between 2019 and 2020 which is the largest proportional drop seen in the UK in a single year since the start of the data series in 1990 [1]. Despite this progress, further action is still required to ensure the global average temperature does not rise by more than 1.5°C when compared with pre-industrial levels. The latest IPCC report predicts that not meeting this target could cause an increase in the ferocity of global floods and fires, the failure of crops and forced migration due to rising sea levels [2].

The UK government has pledged to reduce UK GHG emissions by at least 80% by the year 2050 [3]. To achieve this, sectors such as transport, energy, industry and domestic must play their part. Currently, the goal for the transport sector is to eliminate the use of internal combustion engine vehicles (ICEVs) and move to electric vehicles (EVs) such as battery electric vehicles (BEVs) or fuel cell electric vehicles (FCEVs). The switch to EVs means that GHGs are not produced directly; however, manufacturing and power supply still need to be taken into consideration. Most of the emissions from an EV are produced during its manufacturing, and combined with a high GHG emitting grid results in marginal differences between EVs and ICEVs [4]. Nonetheless, more recent comparative studies showed that BEVs produced 35-50% of the GHG emissions over their life cycle when compared with their ICEV counterpart; factoring in current and future predicted grid supply sources [5, 6]. Moreover, the UK government has a target of 2035 for the energy sector to be only reliant on clean energy, subject to security of supply [7]. One of the fundamental limitations of renewable clean sources is their dependence on external factors such as light intensity or wind speed. Therefore, during high production times, surplus energy must be stored in preparation for when the demand is greater than the supply. Additional storage infrastructure needs to be built alongside new clean energy plants for this to be a viable option. Unfortunately, this additional storage increases the cost of harnessing renewable energy sources; however, the rising popularity of BEVs is a potential solution to reducing this cost. Essentially, BEVs are large battery on wheels, so a bidirectional charger can enable a vehicle to store energy for later use [8]. The BEV is said to be in grid to vehicle (G2V) mode while charging and in vehicle to grid (V2G) mode when supplying power to the grid. It is estimated that personal vehicles are only active for 10% of the day; therefore, these BEVs could be utilised for grid applications for the other 90% [9]. This use of BEVs could also be financially beneficial for the owner as they could be compensated for their participation, with one trial conducted in the UK seeing participants earning as much as £725 in a year [10]. Alternatively, the vehicle could be used as a house battery system to help increase self-sufficiency, especially when paired with rooftop solar panels [8]. This technology is not far off what is currently a reality with smart charging, where BEVs are charged during off-peak times at reduced costs. V2G would take this a step further and allow the owner to sell back to the grid when demand is higher. A few obstacles in the adoption of this technology are the price of EVs, charging infrastructure across the country and lack of global technological standardisation.

Currently, there is a split in the EV market where manufacturers like Hyundai, Audi and Porsche have moved to an 800V EV architecture while others have stayed with the conventional 400V architecture. Moving to an 800V architecture is the next logical step for a BEV as it can offer better charge times at fast charging stations. For example, Porsche claim that their Taycan model can be charged from 5% to 80% in 22.5 minutes [11]. Additional benefits of a higher voltage system include: smaller charging currents which reduce overheating and allow better power retention; smaller cable sizes which reduce raw materials and thereby subsequent costs; reductions in the overall weight of vehicles resulting in increases in both their range, acceleration and energy savings [12–14].

Based on these current trends, the focus of this report will be the design and implementation of a bi-directional charger for an 800V EV architecture. This report will be split into five sections: the proposed charger topology for the model; the design of the G2V mode of the charger; the design of the V2G mode of the charger; the operation of the devised control systems of the charger; the performance of the model and closed-loop controllers.

2 Proposed Charger Topology

In this report, the charger was designed to work in a domestic environment and therefore limited by the single phase grid supply seen in most UK houses. In addition, the charger will have a type-2 outlet, which means the maximum output power would be around 7.2-7.4kW [15,16]. Furthermore, the topology of the charger followed a similar design structures seen in [17–19].

Figure 1 displays the proposed charger topology, consisting of six IGBTs, two inductors, two capacitors, a switch and a battery. An ideal AC voltage source, with a peak voltage of 230V and frequency of 50Hz, was used to model a single phase grid supply. An AC/DC converter, consisting of four IGBTs connected in an H-bridge configuration, was positioned after the grid source. The AC/DC converter acts as a rectifier in G2V mode and an inverter in the V2G mode. A DC-link capacitor was placed directly after the AC/DC converter to smooth any current waveforms in both operation modes. Finally, at the back end of the charger was a C-class chopper comprising of two IGBTs, an inductor, a capacitor and the battery itself. The chopper allows current flow in a positive and negative direction and can either act as a buck converter while in G2V or a boost converter while V2G. There was also an inductor, L_{AC}, positioned after the AC source which had three objectives: in G2V mode, the inductor was utilised to boost the rectified voltage; while its purpose in V2G mode was to reduce harmonic behaviour seen in the current; finally, it also made the AC source less ideal, which is more realistic.

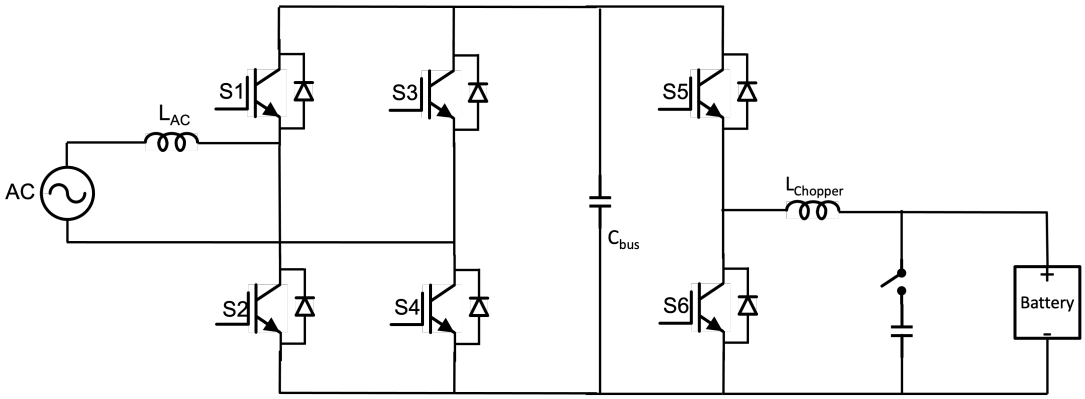

Figure 1: Complete circuit diagram of the designed charger

3 Grid To Vehicle Design

3.1 Charging Topology

This section of the report was focused on the theory and design of the charger while in G2V mode. For this mode, the AC/DC converter acted as a controlled boost rectifier, converting alternating current (AC) to direct current (DC). A boost rectifier takes this a step further by increasing the output voltage of the rectifier. While at the back end, the C-class chopper acts as a buck converter which decreases its input voltage. The AC source was used to mimic a single phase grid source, V_{Grid}, with a peak voltage of 230V and a frequency of 50Hz. The G2V mode of the charger aimed to convert the grid's power into a form that was acceptable for the battery.

3.2 Rectification

The first stage in the charging process is to convert the AC signals produced by the grid to DC signals so that the battery can charge effectively. To properly achieve rectification current should only be travelling one way through the load, and the ripple in the current should be so small that it can be assumed to be constant.

3.2.1 Basic Rectifier

Figure 2a shows a diode in series with an AC voltage source and a resistor; this is a simple way to achieve rectification. Current can only flow through a diode in one direction due to its bias; therefore, current can only enter through one side of the load. For the case in figure 3a, only the positive half of the cycle is allowed to flow around the circuit, while the negative half is blocked by the diode's bias. This process is called half wave rectification given by the waveforms produced, this waveform is displayed in figure 3a. This rectification process is limited by the blocking of the negative half of the current cycle, which means that the power delivery from the source is severely limited.

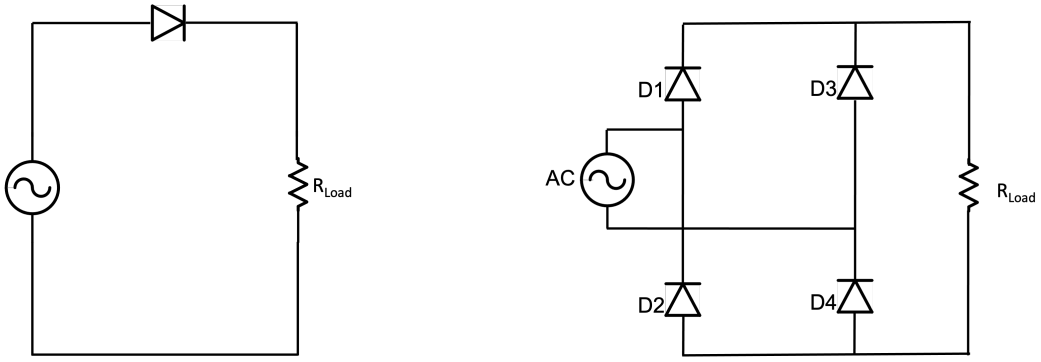

(a) Half wave rectifier **(b)** Full wave rectifier

Figure 2: Circuits diagrams of uncontrolled rectifiers

A full wave rectifier overcomes the limitations of a half wave rectifier and can allow the load to experience the full power of the AC voltage source. This type of rectifier consists of four diodes and the topology is shown in Figure 2b. Using this configuration, the current in the positive half of the cycle flows out of the source and into D1, through the load and back into the source via D4. During the negative half of the cycle, the current flowed out of the source and into D3, where the current then travels through the load and returns to the source via D2. This configuration manipulated the negative half of the current cycle so that it only flowed into the positive end of the load. However, the full wave rectifier can be improved by the addition of a capacitor. Figure 3c displays the effect of the addition of this capacitor in the circuit. Without the capacitor, the average output voltage, V_{dc}, of the rectifier was limited to 63.7% of the peak AC voltage as shown in (1) [20]. The addition of the capacitor smooths the current and voltage waveforms so that they appear DC; this ensured there was effective power transfer.

$$V_{dc} = \frac{2V_{peak}}{\pi} = 0.637V_{peak} \tag{1}$$

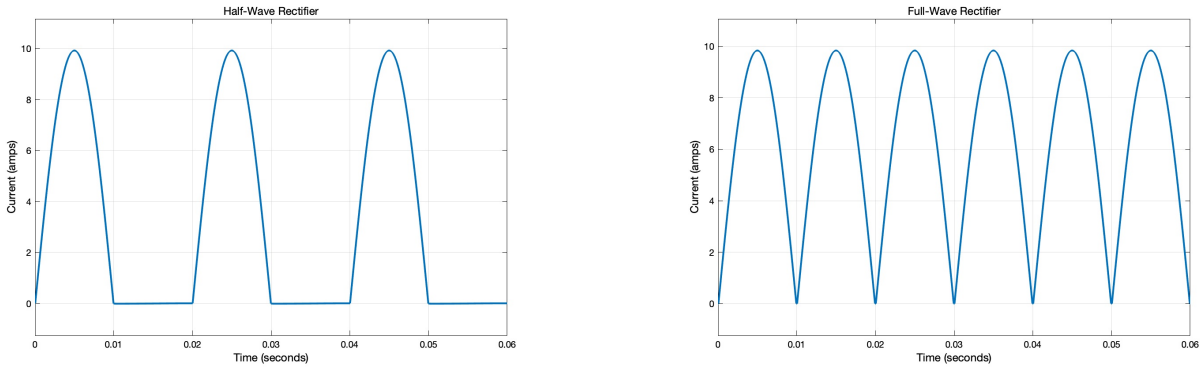

(a) Half-wave rectifier **(b)** Full-wave rectifier

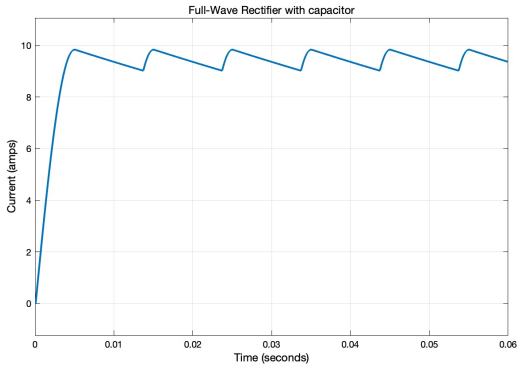

(c) Full-wave rectifier with capacitor

Figure 3: Current waveforms of uncontrolled rectifiers

The diode was previously assumed to be ideal; however, they are not perfect in practice. Figure 2a shows one of the non-ideal behaviours of diodes. Diodes have a latching voltage, usually around 0.7V, that the source must

overcome before the diode can become forward biased. Furthermore, the diode has a reverse recovery current during turn-off for a small amount of time which excess carriers must be swept out of the diode before it can block a negative polarity voltage [21]. In most applications, the characteristics of the diodes do not effect the converters.

Both the half wave and full wave topologies were variants of an uncontrolled rectifier. They are a simple and cheap way of converting AC to DC signals with little to no complexity [21]; however, this rectification process does not allow any control over the voltage or current seen on the other side of the converter, making the potential system very inflexible.

3.2.2 Controlled boost rectifiers

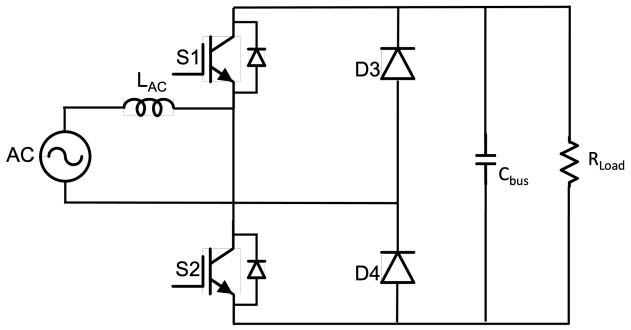

Figure 4: Circuit diagram of a controlled boost rectifier

A controlled rectifier overcomes the limitations of the uncontrolled versions by having the ability to control the output voltage. This variant was constructed by swapping the diodes with four IGBTs and switching pairs of (S1&S4) and (S2&S3). However, it was not essential to have D3 and D4 replaced as the addition of IGBT S1 and S2 can work. By using the switching principles provided in [22] and the addition of an inductor, the controlled rectifier can also boost the output voltage of the converter; therefore, the converter will act as a controlled boost rectifier. The inductor gains charge in the positive half of the current cycle through the switching of S2. While S2 was on, the current flowed from the source to the inductor and back to the source via S2 and D4. The inductor stores charge while current flows like this. Alternatively, when in its off state, current will flow through the inductor from the source, out of the diode in S1, before heading back into the source via D4. The inductor used its stored charge to keep the current flow the same, which results in a higher output voltage. Figure 5 shows an equivalent circuit of the converter when S2 is off.

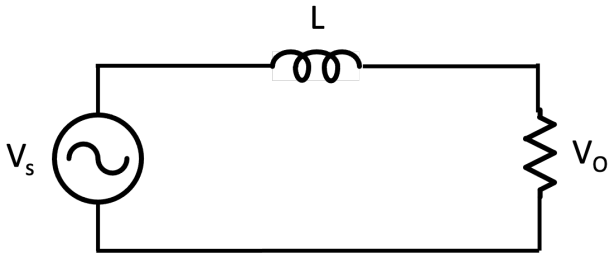

Figure 5: Equivalent circuit when S2 is switched off

Using KVL, the equivalent circuit can be seen in:

$$V_L = L\frac{di}{dt} = V_s - V_o \tag{2}$$

where V_s is the source voltage, V_L is the voltage of the inductor L and V_o is the output voltage. When S2 was switched off, a decrease in current could be seen which was due to the new current path taken. The negative change in current caused a voltage to be induced in the inductor that can be used to boost the output voltage.

The same switching principles are applied to S1 during the negative half of the cycle; furthermore, D3 and the diode in IGBT 2 were used for current paths around the circuit.

3.3 Pulse Width Modulation

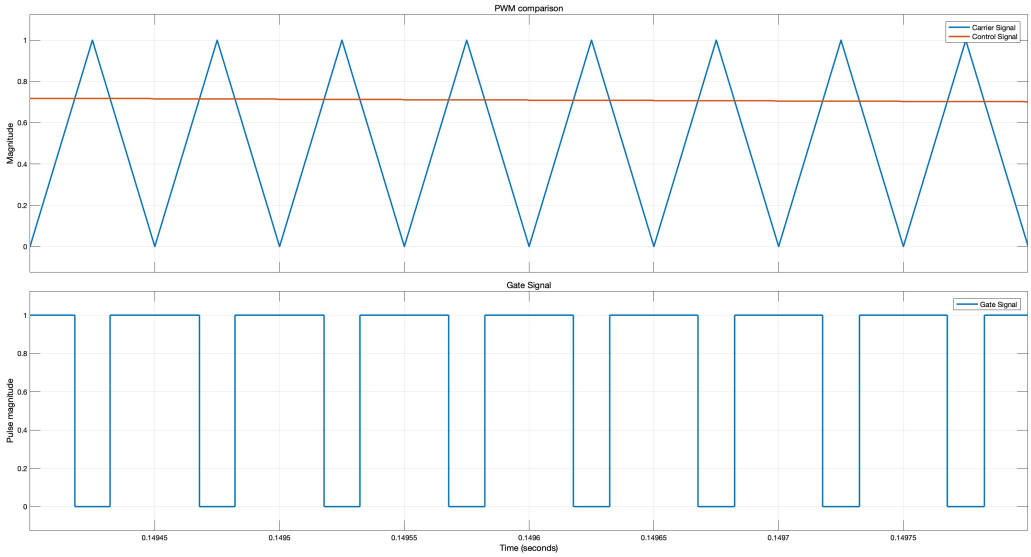

Figure 6: PWM comparison and gate signals

PWM is a way of controlling the signals sent to the switches. It works by the comparison of a control and carrier signal. Usually, the carrier signal is a repeating sequence like a triangular or saw-tooth wave and will have a frequency of the desired switching frequency. It is advised that the carrier signal frequency is at least twenty times larger than that of the control signal for PWM to work effectively. An on-signal is sent to the switch when the control signal is larger than the carrier signal as detailed in figure 6. When the carrier signal is larger than the control signal, the switch receives an off-signal and opens. The control signal must be saturated between the carrier signal to achieve the desired switching. The duty cycle, D, of the converter is the ratio of the on-time, t_{on}, to the total time, T, of one switching cycle.

$$D = \frac{t_{on}}{T} \tag{3}$$

3.4 DC-DC Buck Chopper

3.4.1 Operation

A buck converter is a DC-DC converter that produces a lower output voltage from its initial input. The lowering of the voltage was achieved through the two phases of the buck converter as shown in figures 7a and 7b. In the charging state, S5 was conducting while S6 was off. Therefore, current flowed from the source to the inductor and battery via S5. The role of $L_{Chopper}$ and $C_{Chopper}$ in this mode was to store charge from the source in preparation for the discharging state. Figure 7b displays the current path for the discharging state. In this phase, S5 and S6 are both turned off; therefore, the current was forced to flow from the inductor to the battery and back via the diode in S6. The role of the $L_{Chopper}$ and $C_{Chopper}$ changed for the discharging state. The inductor tried to keep a similar current flow as the previous phase and used its stored charge to do so. The capacitor's role was to reduce any ripples in the voltage and current so that smoother waveforms are seen across the load.

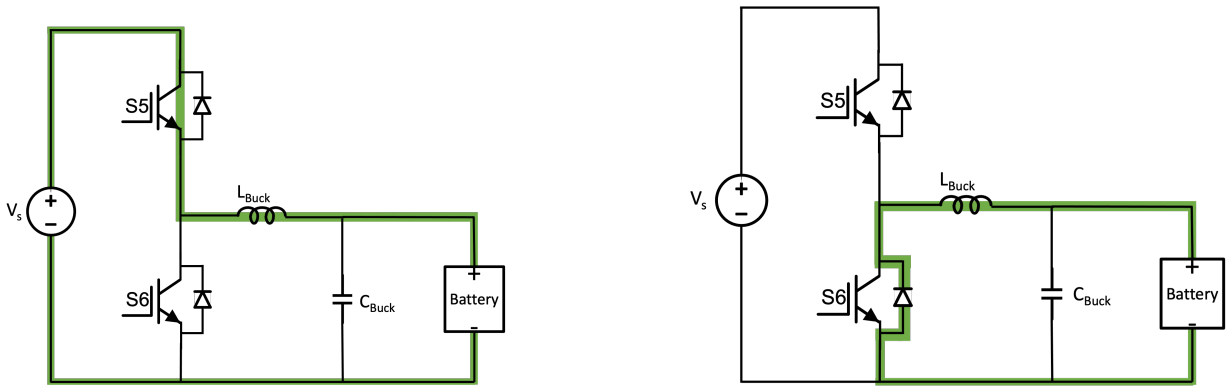

(a) Charging state **(b)** Discharging state

Figure 7: Buck converter states

3.4.2 Duty Cycle and Component Sizing

A buck converter operation is controlled by its duty cycle, D, and the sizing of its components. The following equations are from [23, 24] and they provide a way of sizing devices for the buck converter.

$$D = \frac{t_{on}}{T} = \frac{V_{Load}}{V_s} \tag{4}$$

$$L_{Chopper} = \frac{V_s - V_{Load}}{2 \cdot \delta i} \cdot DT \tag{5}$$

$$C_{Chopper} = \frac{\delta i}{8 f_s \delta V_{out}} \tag{6}$$

The relationship between the duty cycle, time and voltage can be seen in (4). In the equation, t_{on} represents the time period for the charging phase, T represents the total time for one switching cycle, V_s is the input voltage and V_{Load} is the output voltage. The inductor, $L_{Chopper}$, was sized using (5). The variable δi represents the ripple current in the circuit, which can be assumed to be 5% of the current. Finally, (6) can be used to size the capacitor $C_{chopper}$. The only additional information needed for this equation was the switching frequency, which was the reciprocal of the switching period. The ripple in output voltage was also assumed to be 5% of the desired voltage. The combination of (4), (5) (6) and the values in table 1 gave the inductor and capacitor a size of 8.649 mH and 0.00723 μF

Variable	**Symbol**	**Value**	**Units**
Input voltage	V_s	1000	V
Output voltage	V_{Load}	800	V
Voltage ripple	-	5	%
Duty cycle	D	0.8	-
Switching frequency	f_s	20	kHz
Switching period	T	5e-5	s
Average battery current	I_{bat}	9.25	A
Current ripple	-	5	%

Table 1: Buck converter variables and values

4 Vehicle To Grid Design

4.1 Power Back Topology

This next section focused on the theory and design of the charger whilst it was in V2G mode. In this mode, the AC/DC converter was operating as an inverter to produce a sinusoidal current that matched the phase of the grid's voltage. The role of the chopper was to act as a boost converter, where the voltage from the battery was stepped up for the DC-link capacitor before being inverted.

4.2 DC-DC Boost Converter

4.2.1 Operating

A boost converter is a switching converter that has the same components as its buck counterpart, but it instead produces a greater output voltage than input [25]. Similarly, the boost converter has two operating phases which are shown in figures 8a and 8b. The on-state for the boost converter occurred when the IGBT S6 was conducting. During this state, current flowed from the source, V_b, and only into the inductor. The purpose of this phase was for the inductor to store energy to prepare for the off-state. The off-state began when S6 was switched off, and the current flowed through the diode in S5 into the capacitor, as shown in figure 8b. The inductor used its previously stored energy to keep the current flowing the same as in the previous state. The energy combination of the inductor and source was what allowed the capacitor to experience a higher voltage than input voltage.

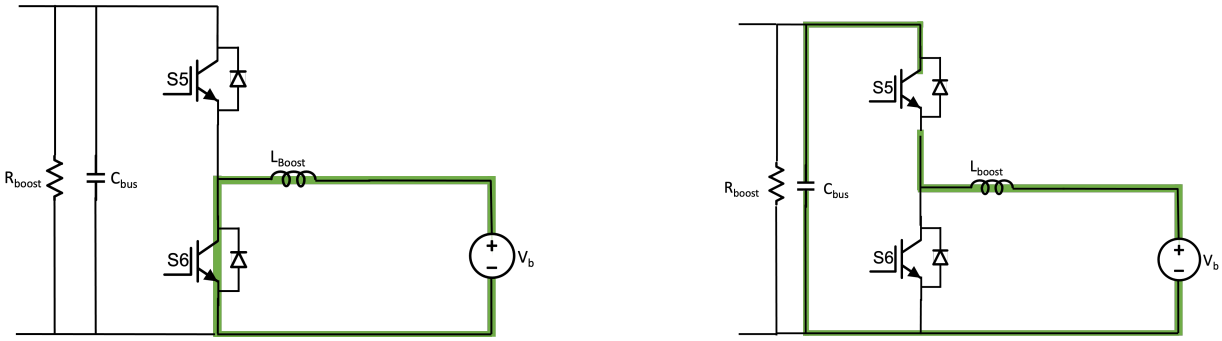

(a) on-state **(b)** off-state

Figure 8: Boost converter states

4.2.2 Component Sizing

Correctly sizing the boost converter's components ensured that it operated properly. To do so the following equations from [23] and [26] were used:

$$D = \frac{V_c - V_b}{V_c} \tag{7}$$

$$L_{Boost} = \frac{V_c}{2R\delta V_c} \cdot DT \tag{8}$$

$$C_{bus} = \frac{V_b}{2\delta i_{Load}} \cdot DT \tag{9}$$

Equation (7) are used to find the duty cycle, D, for the boost converter. The equation uses the output voltage, V_c, and input voltage, V_b, to find the duty cycle. The inductor size, L_{Boost}, was found using (8). Finally, (9) was used to size the DC-link capacitor, C_{bus}. The use of these equations and the parameters specified in table 2 gave an inductor and capacitor size of 8 mH and 1 μF.

Variable	Symbol	Value	Units
Input voltage	V_b	800	V
Output voltage	V_c	1000	V
Voltage ripple	-	5	%
Duty cycle	D	0.2	-
Switching frequency	f_s	20	kHz
Switching period	T	5e-5	s
Average Load current	i_{Load}	10	A
Current ripple	-	5	%

Table 2: Boost converter variables and values

4.3 Inverter

An inverter's objective is to convert DC signals into AC signals whose magnitude and frequency are controllable from the DC input [21]. A half bridge and full bridge inverter can be seen in figures 9a and 9b. It is easier to understand the principles of half bridge inverter than a full bridge inverter, these principles then can be applied to a full bridge inverter as it consists of two half bridge inverters. Full bridge inverter can deliver twice the output voltage than a half bridge inverter. Therefore, for the same power supply, the output current can be one half of that in a half bridge inverter [21]. It is important to realise that the full bridge inverter's topology is identical to the controlled boost rectifier discussed earlier. Therefore, no physical alterations to the circuit are required for power to flow both ways, only the method by which the devices switch.

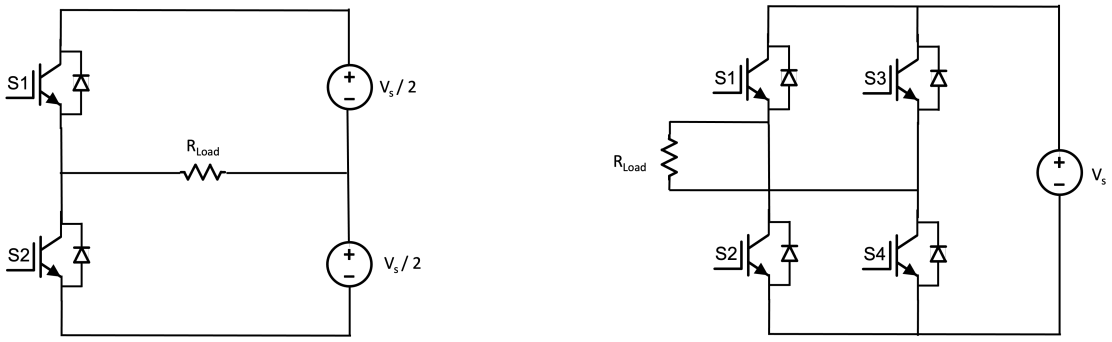

(a) Single phase half bridge inverter **(b)** Single phase full bridge inverter

Figure 9: Inverter topologies

4.3.1 Sinusoidal Pulse Width Modulation

PWM was already discussed in the previous section; however, a slightly more complex variant called sinusoidal pulse width modulation (SPWM) was used on the charger's inverter. SPWM aids the inverter's goal of a controllable output magnitude and frequency. Like PWM, SPWM utilises the comparison of a modulation and carrier signal. The carrier signals was a repeating sequence with a frequency of the desired switching frequency. However, the modulation signal is what distinguishes the two techniques. Now, the modulation signal used will be a sinusoid with the desired characteristics of the output signal. The output of the inverter using SPWM is dependent on the amplitude and frequency modulation ratio.

$$m_f = \frac{f_{tri}}{f_{mod}} \tag{10}$$

The frequency modulations ratio, m_f, can be seen in (10). It represents the ratio of the frequencies of the carrier and modulation signals. Ideally, the size of m_f should be large to assume that the modulation signal is roughly constant within the carrier signal cycle.

$$m_a = \frac{\hat{V}_{mod}}{\hat{V}_{tri}} \tag{11}$$

The amplitude modulation ratio is defined as the ratio of the peak amplitude of the modulation and carrier signals as shown in (11). This ratio is used to control the output voltage of the inverter.

The switches in the half bridge inverter, shown in figure 9a, were controlled by the signals produced by the

comparison of the modulation and carrier signals. If the modulation signal is larger than the carrier, (12) applies, and the converse is true for (13).

$$V_{mod} > V_{trig}, \qquad S1 \; is \; on, \qquad v_{output} = \frac{V_s}{2} \tag{12}$$

$$V_{trig} > V_{mod}, \qquad S2 \; is \; on, \qquad v_{output} = -\frac{V_s}{2} \tag{13}$$

where v_{output} is the output of the inverter and V_s is DC input voltage. S1 and S2 are never simultaneously on because of how the switching works. This means that the output voltage will either be $+\frac{V_s}{2}$ or $-\frac{V_s}{2}$. The comparison for switching and output voltage is shown in figure 10. The dotted voltage line represents the average output voltage of the inverter v_o. The frequency of v_o matches that of the modulation signal and the peak amplitude, $\hat{V}_o$, can be found using (14).

$$\hat{V}_o = m_a \frac{V_s}{2} \tag{14}$$

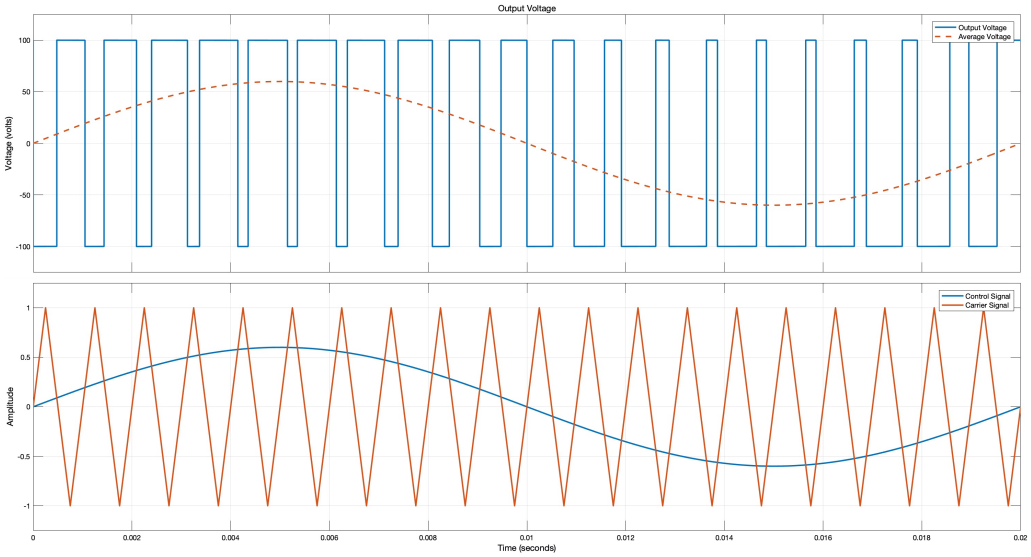

Figure 10: Voltage output and modulation waveforms of a half bridge inverter

4.3.2 Bi-polar v Uni-Polar Switching

The full bridge inverter in figure 9b can either use a uni-polar or bi-polar switching scheme. The bi-polar method uses switching pairs of (S1 & S4) and (S2 & S3). These pairs were switched using the same method as the half bridge inverter where the voltage can either be $+V_s$ or $-V_s$. Similarly, for a bi-polar full bridge converter, the peak output voltage could be found using (15)

$$\hat{V}_o = m_a V_s \tag{15}$$

Uni-polar differs from bi-polar switching by allowing each switch to receive its own gate signals. S1 and S2 are switched using a comparison of v_{mod} and v_{trig} while, S3 and S4 are switched using the comparison of $-v_{mod}$ and v_{trig}. The conditions for the switching scheme can be seen in (16) and (17).

$$\begin{aligned} V_{mod} > V_{trig}, \qquad & S1 \; is \; on, \qquad v_{ao} = V_s \\ V_{trig} > V_{mod}, \qquad & S2 \; is \; on, \qquad v_{ao} = 0 \end{aligned} \tag{16}$$

$$\begin{aligned} -V_{mod} > V_{trig}, \qquad & S3 \; is \; on, \qquad v_{bo} = V_s \\ -V_{trig} > V_{mod}, \qquad & S4 \; is \; on, \qquad v_{bo} = 0 \end{aligned} \tag{17}$$

Each half bridge inverter in figure 9b can be thought of as an inverter leg. The output voltage of leg 'a' was v_{ao} and similarly for leg 'b' it was v_{bo}. (18) displays the final output voltage of the inverter.

$$V_{output} = v_{ao} - v_{bo} \tag{18}$$

The voltage output of an inverter that uses a uni-polar switching scheme can either be $+V_s$, $-V_s$ or 0. Some advantages of the uni-polar method include reduced switching losses, better efficiency and lower total harmonic distortion [27]. Therefore, uni-polar switching was used on the AC/DC converter when it was acting as an inverter.

5 Controller Design

5.1 Rate Transition Blocks

The use of a rate transition block was not vital in the key operations of the controllers; however, its inclusion meant that the simulations ran faster due to reduced memory requirements. The purpose of the block is to handle the transfer of data from two blocks operating at different rates [28]. In the case of the controllers, the block held the output for one switching cycle and only after the cycle did the output change.

5.2 Proportional + Integral Controller (PI)

All of the control systems for the bi-directional charger used a PI controller. The controller aimed to minimise the error between the reference and measured signal. The proportional term relates to the responsiveness of the control system, while the integral term is associated with the elimination of any steady-state error. Correct tuning of the controller would result in a fast transient response, with minimal overshoot and zero steady-state error. A disadvantage of this controller was that the system would become unstable if gains were chosen incorrectly. The gains of the system were selected via a trial and error method; therefore, the final gains used may not have been the optimal choice but offer a satisfactory response. Finally, the derivative term of the system was neglected due to the nature of power electronic systems. The high switching frequencies of PWM tend to generate a lot of noise, which could be amplified by the derivative term and cause the system to become unstable.

5.3 Buck and Boost

The control structure of the buck and boost controllers were very similar, and therefore it is only necessary to explain how one worked. The following text discusses how the controller of the buck converter worked. Figure 11 displays the block diagram of the buck converter controller. The controller works by finding the error between the reference and measured load voltage. This error is then normalised by the reference voltage and fed into the PI controller, which then produced the desired duty ratio for the converter. The value was then saturated between one and zero for PWM to work effectively for reasons discussed previously. The output of the control system was the gate signal for S5.

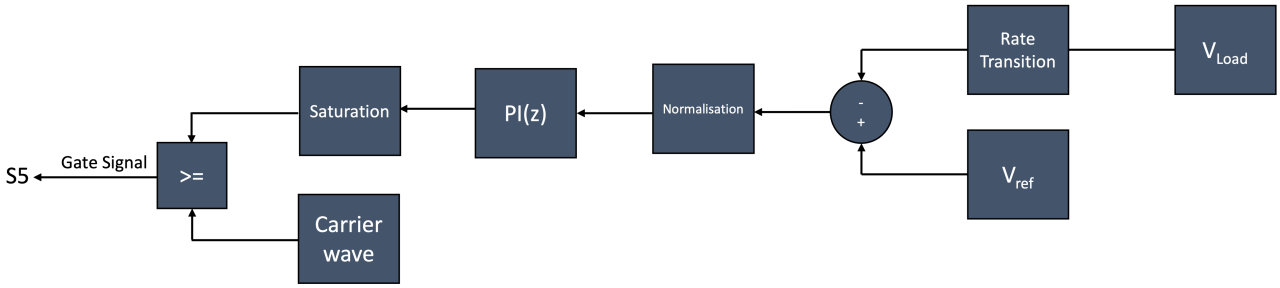

Figure 11: Block diagram of buck converter controller

5.4 Rectifier

The controller for the rectifier had two main objectives. Firstly, it had to produce the desired voltage, V_{ref}, across the DC-link capacitor. Secondly, it had to ensure that the current was in phase with the voltage; this was necessary to ensure that the system worked close to unity power factor. One potential method that could have been selected was a hysteresis control structure like in [22]. This controller worked by setting a reference signal with a predetermined hysteresis band. The output of the hysteresis controller sent gate pulses to the switches in order to maintain the actual current in the reference current's band [29]. The main disadvantage of this method was that the switching frequency was not constant, which is not ideal for electrical machines as they are variable frequency applications [30].

The controller that was integrated into the Simulink model was based on [31]. Figure 12 displays a block

diagram of the rectifier control system. The controller worked by finding the error between the reference and actual voltage. The PI controller used the error to create a reference current which was multiplied by the normalised grid voltage; this created a reference sinusoidal current that was in phase with the grid. The signal was then subtracted by the measured grid current which was then compared to a carrier signal for PWM. This comparison drove the switching of S1 and S2.

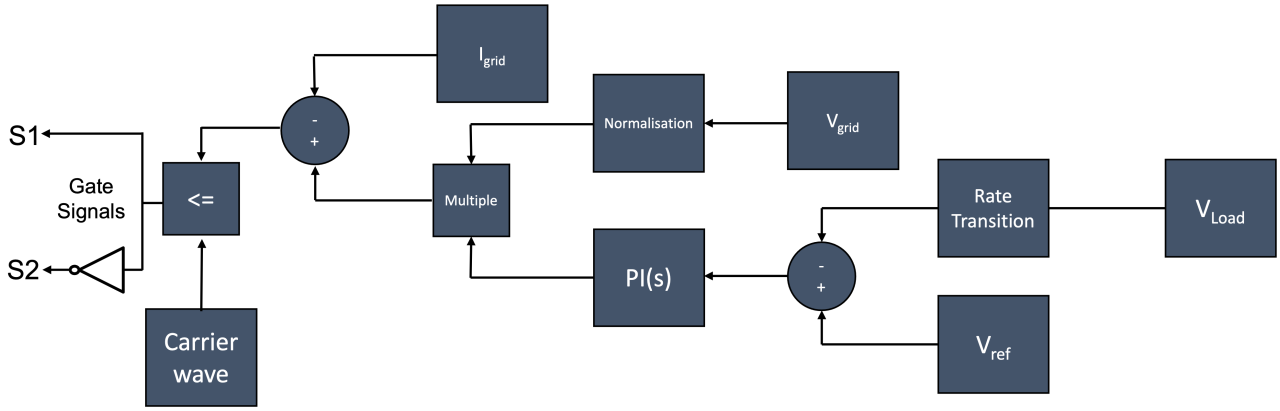

Figure 12: Block diagram of rectifier controller

5.5 Inverter

The inverter used a uni-polar switching scheme, which meant that S1, S2, S3 and S4 received their own switching signals. The controller for the inverter used a more robust method to achieve grid synchronisation than seen in the rectifier's control strategy. The inverter needed to produce an output current that was 180 °out of phase with the voltage. This phase difference meant that the charger's power output was negative, and therefore the charger was sending power back to the grid. The phase of the current was controlled by the manipulation of the direct, i_d, and quadrature, i_q, currents. The direct current is associated with the active power of the system, whilst the quadrature current is related to reactive power. Grid synchronisation was achieved by getting i_q as close to zero and setting a negative value for i_d.

5.5.1 Park Transformation

Three phase systems use Park and Clarke transformations in order to move from the abc reference frame to the dq rotating frame. The Clarke transformation is not necessary for single phase systems. As it converts the time domain components of the three phase system to two components in the $\alpha\beta$ frame. The Park transformation converts these $\alpha\beta$ signals into the dq frame, which can then be used to control i_d and i_q [32]. The Park transformation can be seen in (19) but will be implemented using the $\alpha\beta$ to dq block in Simulink as shown in figure 14.

$$\begin{bmatrix} i_d \\ i_q \end{bmatrix} = \begin{bmatrix} cos(\theta) & sin(\theta) \\ -sin(\theta) & cos(\theta) \end{bmatrix} \begin{bmatrix} i_\alpha \\ i_\beta \end{bmatrix} \tag{19}$$

The Park transformation works by rotating two orthogonal signals, $\alpha\beta$, at the fundamental frequency θ. In this rotating frame, the resulting dq signals will be constant for sinusoidal frequencies at the same θ as shown in figure 13 [33] . Since the Park transformation requires two sinusoidal signals to transform into the dq frame, the single signal in the system was delayed by 90° to produce pseudo alpha-beta signals. The original signal will be the α signal, and the delayed signal will be β.

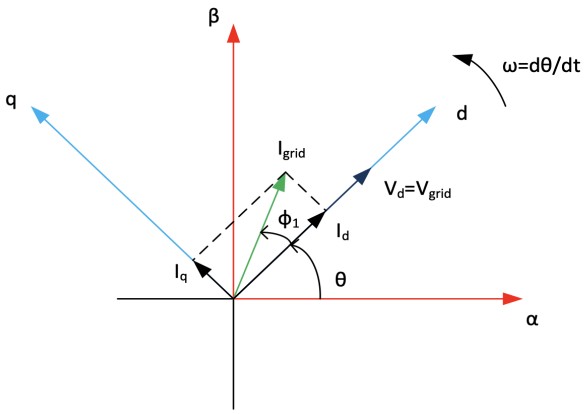

Figure 13: alpha-beta (stationary) and dq (rotating) reference frames [34]

5.5.2 Current Control

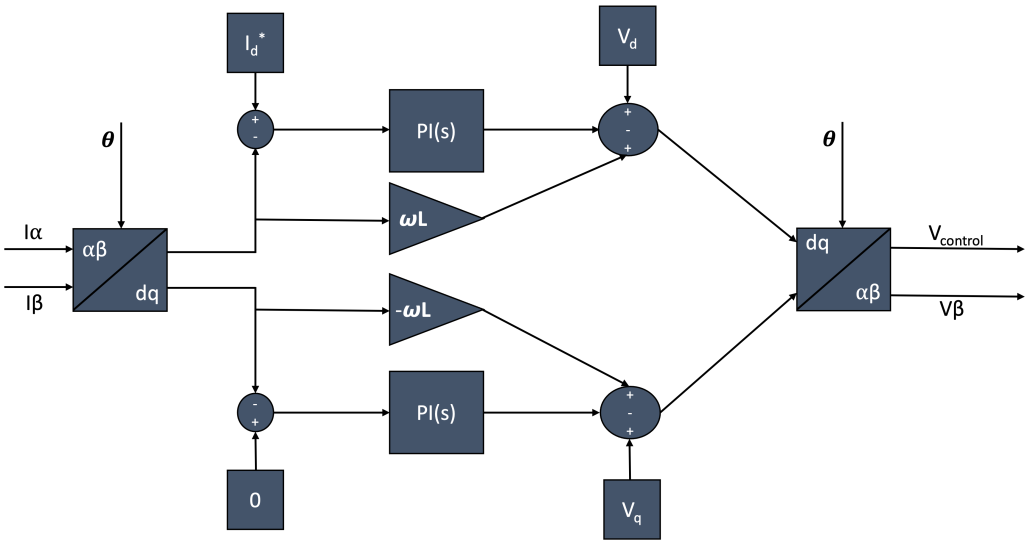

Figure 14: Current control of inverter

Figure 14 shows the block diagram of the current controller for the inverter. This control system was modified from [18, 35] and provided a way to control the active and reactive parts of the power. The first stage of the controller worked by transforming the $\alpha\beta$ current signals to the dq reference frame. To do this, three input signals were needed: the α signal (which is just the output current), the β signal (which is a 90°delay of the output current) and the fundamental frequency. The value for θ was found using the relationship shown in (20). In the actual system, θ was found by the system shown in figure 15, which tracked θ and provided the values for the direct and quadrature parts of the voltage, which will be used later when decoupling the dq currents. Once the currents have moved to the dq frame, they are both compared to their reference currents. The reference signal for i_q was 0; this had the aim to minimise the reactive power in the system. These signals are then passed through a PI controller and decoupled using methods discussed in [35]. The signals were then moved back to the $\alpha\beta$ frame using the inverse Park transformation. The output α signal was then used as the control signal for the uni-polar switching scheme.

$$\theta = \arctan(\frac{\beta}{\alpha}) \tag{20}$$

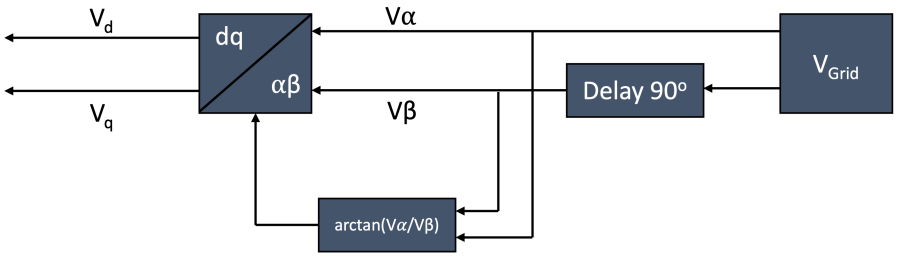

Figure 15: Fundamental frequency tracker

5.6 Dead-Time Effect

It was assumed that the switches worked ideally; however, this is not the case in an actual system. These switching devices tend to turn on quicker than they turn off and therefore need to include a period of time where both switches are off. This period of time is called dead-time and is a temporary loss of control [35]. Dead-time could affect the performance of the system and generate undesirable harmonics; however, the exclusion of it could lead to the system becoming unsafe and could have disastrous consequences for the devices in question [21]. The dead-time effect has a greater influence in systems with higher switching frequencies.

6 Simulations

Figure 16 shows the designed Simulink model of the charger. The Simulink model was split into three sections: the grid, AC/DC converter and the C-class chopper. Figures 17 and 18 display the control systems within the Simulink model. Currently, the controllers need to be commented out for the system to work, as they would interfere with each other. Table 3 shows parameters for the Simulink model while table 4 shows the gains for the PI controllers. The size of the two capacitors were increased from the theoretical design to reduce the ripple in the current. The size of the current ripple is inversely proportional to the size of the capacitor, and therefore, by increasing capacitance size, the ripple in the current would reduce.

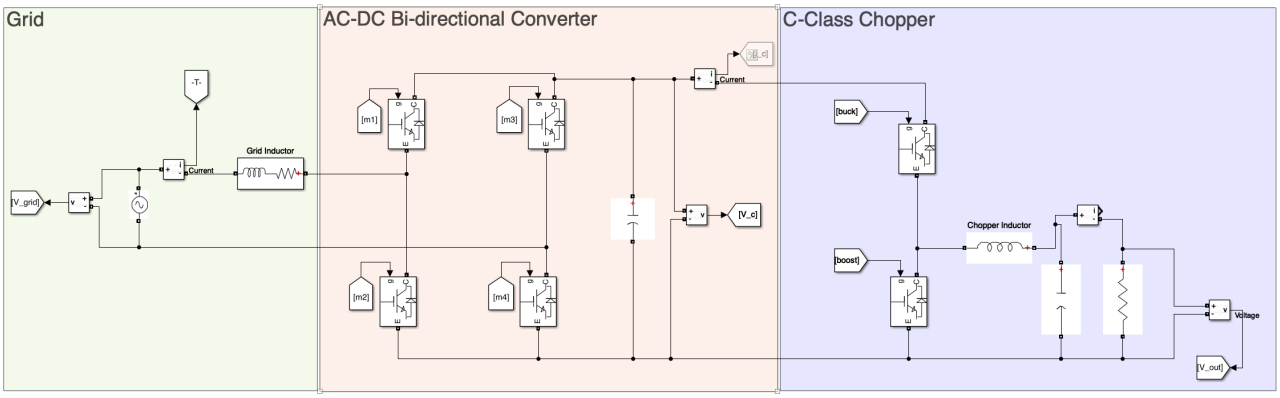

Figure 16: Simulink model of the charger in V2G mode

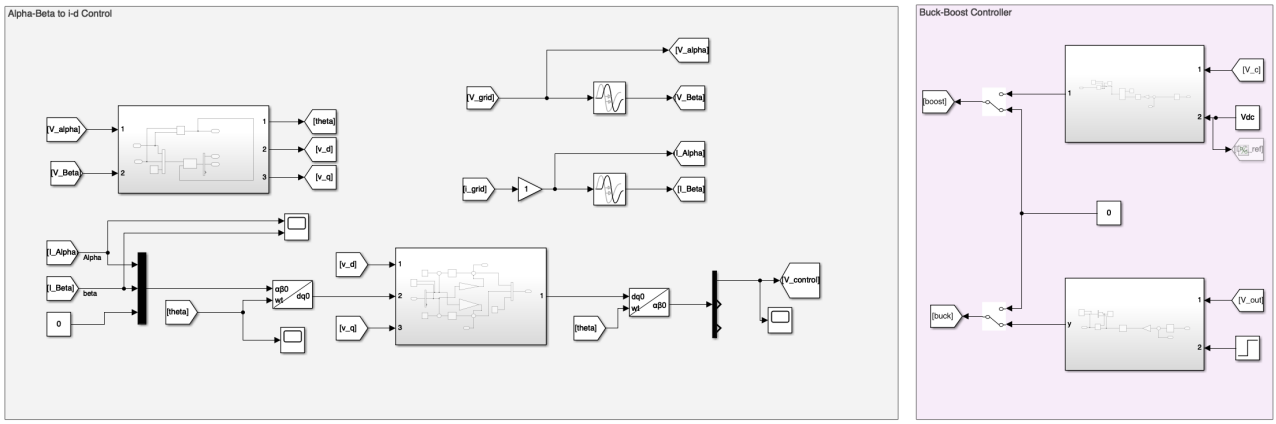

Figure 17: Controllers for the designed Simulink model (1)

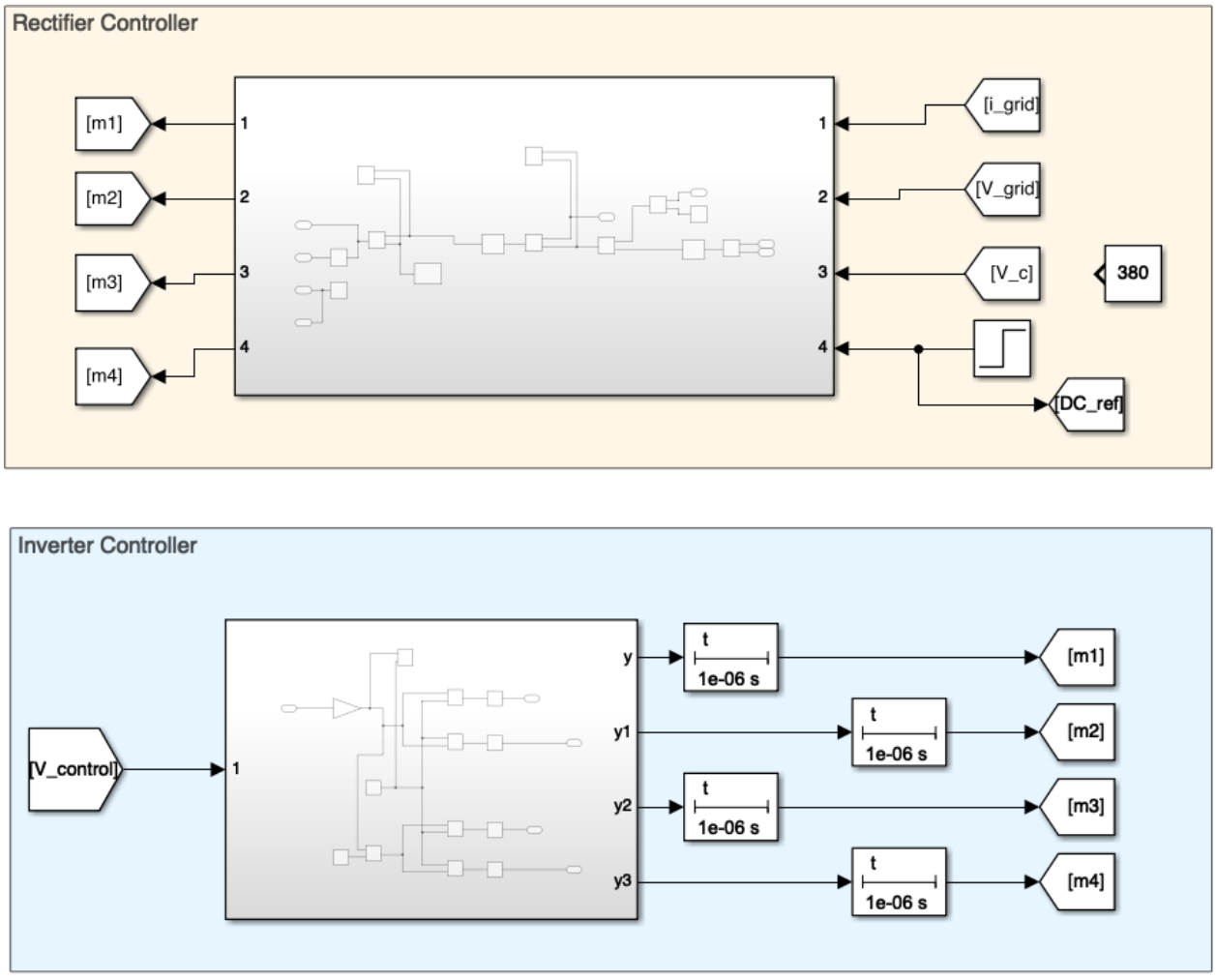

Figure 18: Controllers for the designed Simulink model (2)

Variable	Symbol	Value	Units
Grid voltage	V_{grid}	230	V
Grid Frequency	f_{grid}	50	Hz
Grid Inductor	L_{AC}	1e-3	H
Grid Resistor	R_{grid}	1e-4	Ω
DC-Link capacitor	C_{bus}	1e-4	F
Chopper Inductor	$L_{chopper}$	8.694e-3	s
Chopper Capacitor	$C_{chopper}$	1.876e-3	F
Switching frequency	f_s	20	kHz

Table 3: Component values for Simulink model

Inverter		**Buck Converter**	
kp_d, kp_q	350, 500	kp	14
ki_d, ki_q	250, 250	ki	16
Rectifier		**Boost Converter**	
kp	0.1	kp	0.1
ki	15	ki	20

Table 4: Controller gains

6.1 G2V mode

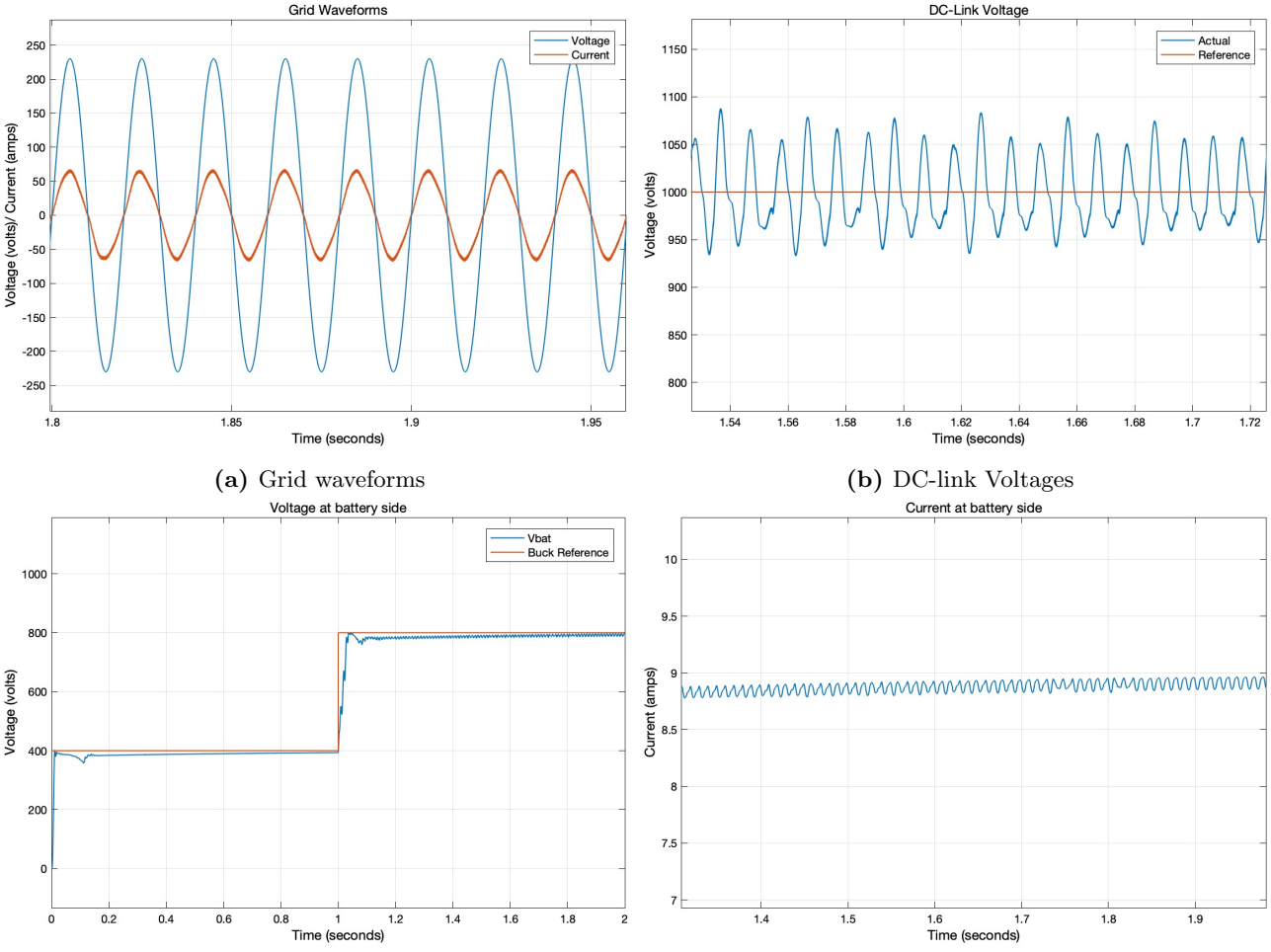

(a) Grid waveforms

(b) DC-link Voltages

(c) Voltage at battery terminal

(d) Current at battery terminal

Figure 19: V2G simulation waveforms

Figure 19 displays the simulation results of the charger while in G2V mode. For simplicity, the battery was modelled using a resistor to check the rectifier and buck converter controllers. The figures 19a and 19b show that the rectifier is working correctly. Since the figure 19a is showing in phase current and voltage, the reactive power of the system has successfully been minimised. However, the current sinusoidal waveform is slightly skewed, which could be caused by the control method used for the rectifier. The ripple in the DC-link voltage was around 7% which was slightly larger than what is desirable. This ripple could be made smaller with more precise tuning, but the output signal was close enough to deem the controller functional.

Figure 19c displays the performance of the buck control system. Initially, the buck converter had a reference signal of 400V and at one second the signal was stepped up to 800V. This result meant that the charger

could work for a 400V architecture if the BEV had the correct hardware. The buck controller had a good settling time, overshoot and rise time; however, the system did have a small steady-state error. The steady-state error would have become insignificant if the simulation was run for longer. Nonetheless, the operation of the buck converter was good, especially since there was no overshoot to potentially cause damage to the battery. Finally, figure 19d shows that the current at the battery terminal can be considered to be DC due to the small ripple. Therefore, the charger is working as designed while in G2V mode.

6.2 V2G mode

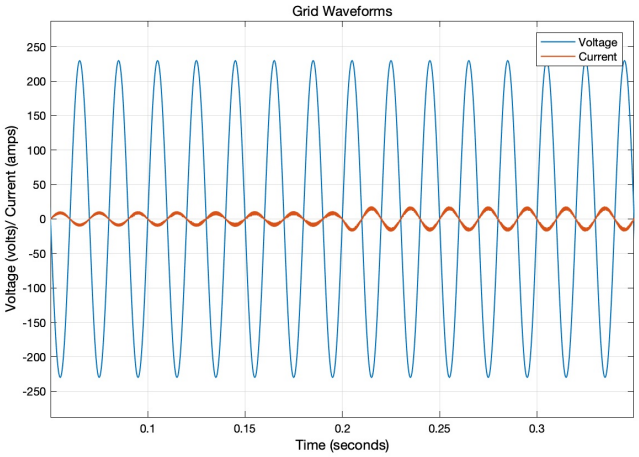

(a) Grid waveforms

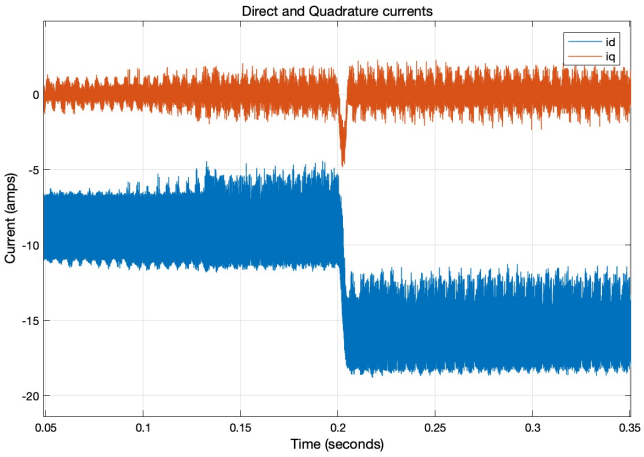

(b) Direct and quadrature currents

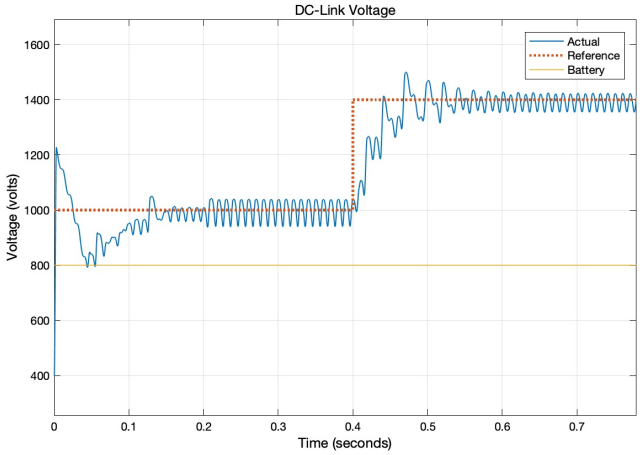

(c) DC-link Voltage

Figure 20: V2G simulation waveforms

Figure 20 displays the simulation results while the charger was in V2G mode. The modelling of the battery was done using a DC voltage source with an output voltage of 800V. In this mode, the chopper was acting as a boost converter, which is demonstrated in figure 20c. The controller reached the desired value but did have oscillatory behaviour; however, it was deemed that the controller was in steady-state. This oscillatory behaviour could be due to the switcher of the inverter as the ripple had a frequency of 25Hz which is half the output waveforms of the inverter. Moreover, the controller had a very good response to a step demand change, as the system rose and settled quickly.

Figure 20a shows the output current and voltage of the inverter. There was a 180° phase difference between the grid voltage and current as intended. From inspection, the inverter and its controller were working. Figure 20b gives a better view of the operation of the inverter controller. The figure shows the values of the direct and quadrature currents for the system. The quadrature current was minimised and can be considered to be held at 0, and the direct current was held at its reference value. Furthermore, the system had a good response to a change in the current demand as shown in figure 20b Therefore, the charger is working as designed while in V2G mode.

7 Conclusion

This report documented the design process of a bi-directional charger that can either work on a 400V or 800V BEV architecture. Two models of the charger were created in Simulink to test the closed-loop control systems, one mode for the G2V and the other for V2G. The buck, boost and inverter controllers worked as intended; however, further work is still needed on the rectifier control system, due to the slightly irregular output. It can be concluded that the controllers for each operation mode work, and therefore the charger model is functional. This technology will become increasingly important in the next few years as we move away from fossil fuels and aim to reduce our GHG emissions. It is important that the foundations for a more sustainable tomorrow are placed as early as possible, as infrastructure takes time to adjust.

8 Future Work

The next step to create a complete model is to include the battery block from Simulink, since the block was excluded for simplicity and to ensure the controllers worked. Once the integration of the battery block is complete, an energy management system (EMS) could be added. Currently, each controller works independently from the other, which means they must be activated or deactivated manually. An EMS would combine all the controllers into one control system, streamlining switching from V2G and G2V mode depending on the demand signal. For example, if +1kW is the demand signal, then the EMS would add that amount of power to the battery. A negative demand signal would put the charger in power back mode and inject the energy back into the grid. Also, the addition of a soft start up system is vital in ensuring that components do not fail due to sudden current or voltage changes. A final addition to the simulation model would be the inclusion of an optimal battery charging strategy. This strategy could work by using constant current charging when charge is low and then switching to constant voltage charging when near completion. The aim of the charging strategy is to preserve battery health and increase its lifespan.

The addition of the battery block, EMS and charging strategy would push everything that could be achieved in the simulation of the charger. For this reason, the next stage of the charger development would be creating a physical model. This model would be a scaled version due to safety; however, the physical model would test the system's safety, provide information about thermal performance of the charger and possibly highlight areas where performance could be improved.

This additional work would complete the designing stage of the charger and therefore the next stage would be the optimisation stage. One of the easier ways to improve the charger performance could be trialling alternative controllers such as PR or Fuzzy Logic. These controllers could reduce the ripple seen across the steady state values for the DC-link voltage or the dq currents. Furthermore, developments may include improving the response time of the control system and modifying the rectifier controller so that the dq currents can be controlled using the same controller approach used in the inverter system.

References

[1] Energy & Industrial Strategy Department for Business. 2020 uk greenhouse gas emissions, final figures. Technical report, National Statistics, Feb 2022.

[2] Climate change 2022: impacts, adaptation and vulnerbility. Technical report, IPCC, Feb 2022.

[3] Renewable generation. https://www.energy-uk.org.uk/energy-industry/renewable-generation.html. Accessed: 2022-22-04.

[4] Hongrui Ma& Felix Balthasar& Nigel Tait& Xavier Riera-Palou& Andrew Harrison. A new comparison between the life cycle greenhouse gas emissions of battery electric vehicles and internal combustion vehicles. In *Energy Policy*, volume 44, pages 160–173, Jan 2012.

[5] Auke Hoekstra. The underestimated potential of battery electric vehicles to reduce emissions. In *Joule*, volume 3, pages 1412–1414, July 2019.

[6] Qinyu Qiao & Fuquan Zhao & Zongwei Liu & Xin He & Han Hao. Life cycle greenhouse gas emissions of electric vehicles in china: Combining the vehicle cycle and fuel cycle. In *Energy*, volume 177, pages 222–233, April 2019.

[7] Energy & Industrial Strategy Department for Business. Net zero strategy: Build back greener. Technical report, HM Government, October 2021.

[8] Jason Svarc. Bidirectional chargers explained - v2g vs v2h vs v2l. https://www.cleanenergyreviews.info/blog/bidirectional-ev-charging-v2g-v2h-v2l, Feb 2022. Accessed: 2022-21-04.

[9] Kang Miao Tan, Vigna K. Ramachandaramurthy, and Jia Ying Yong. Bidirectional battery charger for electric vehicle. In *2014 IEEE Innovative Smart Grid Technologies - Asia (ISGT ASIA)*, pages 406–411, 2014.

[10] Ofgem. Case study (uk): Electric vehicle-to-grid (v2g) charging. https://www.ofgem.gov.uk/publications/case-study-uk-electric-vehicle-grid-v2g-charging, July 2021. Accessed: 2022-25-04.

[11] INSIDEEVs. Porsche taycan (93 kwh battery) fast charging analysis: Very good. https://insideevs.com/news/512344/porsche-taycan-fast-charging-analysis/, June 2021. Accessed: 2022-25-04".

[12] ET editorial staff. 800v systems in evs enable longer ranges, faster charging. https://eandt.theiet.org/content/articles/2021/02/800v-systems-in-evs-enable-longer-ranges-faster-\newlinecharging/, Feb 2021. Accessed: 2022-25-04".

[13] Iman Aghabali, Jennifer Bauman, Phillip J. Kollmeyer, Yawei Wang, Berker Bilgin, and Ali Emadi. 800-v electric vehicle powertrains: Review and analysis of benefits, challenges, and future trends. *IEEE Transactions on Transportation Electrification*, 7(3):927–948, 2021.

[14] David Jolley. Shifting to 800-volt systems: Why boosting motor power could be the key to better electric cars. https://cordis.europa.eu/article/id/429197-shifting-to-800-volt-systems-why-boosting-\newlinemotor-power-could-be-the-key-to-better-\newlineelectric-car, Feb 2021. Accessed: 2022-26-04.

[15] Energy Solutions, United Kingdom. *GUIDE TO ELECTRIC VEHICLE CHARGING.*

[16] Audi e-tron gt podpoint. https://pod-point.com/guides/vehicles/audi/2021/etron-gt. Accessed: 2022-14-04.

[17] Hugo Neves de Melo, João Pedro F. Trovão, Paulo G. Pereirinha, Humberto M. Jorge, and Carlos Henggeler Antunes. A controllable bidirectional battery charger for electric vehicles with vehicle-to-grid capability. *IEEE Transactions on Vehicular Technology*, 67(1):114–123, 2018.

[18] Xiaoqiang Guo, Jian Li, and Xiaoyu Wang. Impact of grid and load disturbances on electric vehicle battery in g2v/v2g and v2h mode. In *2015 IEEE Energy Conversion Congress and Exposition (ECCE)*, pages 5406–5410, 2015.

[19] Gyu-Yeong Choe, Jong-Soo Kim, Byoung-Kuk Lee, Chung-Yuen Won, and Tea-Won Lee. A bi-directional battery charger for electric vehicles using photovoltaic pcs systems. In *2010 IEEE Vehicle Power and Propulsion Conference*, pages 1–6, 2010.

[20] Full wave rectifier. https://www.electronics-tutorials.ws/diode/diode_6.html. Accessed: 2022-28-03.

[21] William P. Robbins Ned Mohan, Tore M. Undeland. *Power electronics - Converters, applications and design Third Edition*. JOHN WILEY and SONS, INC, 2003.

[22] Seshadri Gopalan. Design and control of single phase pwm rectifier using two igbt. In *International Journal of Advanced Research in Electrical, Electronics and Instrumentation Engineering*, volume 4, pages 5694–5699, 2015.

[23] Mário A. Silva, João P. Trovão, Pereirinha, and Paulo G. Implementation of a multiple input dc-dc converter for electric vehicle power system. In *Proceedings of the 2011 3rd International Youth Conference on Energetics (IYCE)*, pages 1–8, 2011.

[24] Brigitte Hauke. Basic calculation of a buck converter's power stage. Technical report, Texas instruments, 8 2015.

[25] Marcelo Godoy Simes and Felix A. Farret. *DESIGNING POWER ELECTRONIC CONTROL SYSTEMS*, pages 83–116. 2017.

[26] S. Padhmanabhaiyappan, R. Karthik, and K. Ayyar. Investigation of controllers for dc-dc boost converter. In *2018 International Conference on Power, Energy, Control and Transmission Systems (ICPECTS)*, pages 306–308, 2018.

[27] Anuja Namboodiri Harshal S. Wani. Unipolar and bipolar pwm inverter. In *International Journal for Innovative Research in Science Technology*, volume 1, pages 237–243, 2014.

[28] Rate transition, mathworks. https://uk.mathworks.com/help/simulink/slref/ratetransition.html. Accessed: 2022-05-04.

[29] Arpit Bohra, Divya Sajeesh, Chintan Patel, and Michael Saldanha. Modulation techniques in single phase pwm rectifier. In *International Journal of Computer Applications*, 2015.

[30] André Veltman. Rik De Doncker, Duco W.J. Pulle. *Advanced electrical drives : analysis, modeling, control*. Springer, New York, NY, 2011.

[31] Arun Kumar Verma, Bhim Singh, and D.T. Shahani. Grid to vehicle and vehicle to grid energy transfer using single-phase bidirectional ac-dc converter and bidirectional dc-dc converter. In *2011 International Conference on Energy, Automation and Signal*, pages 1–5, 2011.

[32] Clarke and park transforms. https://uk.mathworks.com/solutions/power-electronics-control/clarke-and-park-transforms.html. Accessed: 2022-16-04.

[33] B. Crowhurst, E. F. El-Saadany, L. El Chaar, and L. A. Lamont. Single-phase grid-tie inverter control using dq transform for active and reactive load power compensation. In *2010 IEEE International Conference on Power and Energy*, pages 489–494, 2010.

[34] Giuseppe Marco Tina and Giovanni Celsa. A matlab/simulink model of a grid connected single-phase inverter. In *2015 50th International Universities Power Engineering Conference (UPEC)*, pages 1–6, 2015.

[35] Sylvain LECHAT SANJUAN. Voltage oriented control of three-phase boost pwm converters. Master's thesis, CHALMERS UNIVERSITY OF TECHNOLOGY, Göteborg, Sweden, 2010.